# *In situ* x-ray study of $Fe_3Al(110)$ subsurface superlattice disordering during oxidation

V. Vonk,* C. Ellinger, N. Khorshidi, A. Vlad, A. Stierle, and H. Dosch
*Max Planck Institute for Metals Research, 70569 Stuttgart, Germany*
(Received 25 June 2008; published 27 October 2008)

We report an *in situ* x-ray investigation of the $Fe_3Al(110)$ surface during oxidation with a special focus on its impact onto the superlattice order. Upon oxidation at $10^{-6}$ mbar of molecular oxygen at a temperature of 573 K, the long-range superlattice order disappears completely in an extended subsurface region, without affecting the surface roughness nor the crystallinity. These findings can be understood by preferential surface segregation of Al in the presence of oxygen. We argue that this unavoidable subsurface disordering process should render these materials more brittle and vulnerable to aggressive environments, which is important for the use of iron-aluminum alloys as structural materials.

DOI: 10.1103/PhysRevB.78.165426 PACS number(s): 68.47.De, 68.35.bd, 61.05.C−

## I. INTRODUCTION

Iron aluminides are promising materials as future lightweight replacements of steel, because of their potentially favorable density-strength ratio, their use in deep draw processes, and for their high-temperature stability.[1] However, in order to be used in high-temperature structural applications it is necessary that a protective oxide scale is formed on the surfaces of these materials to prevent them from further corrosion. Usually, selective oxidation of only one of the elements in binary alloys takes place, like in the case of NiAl,[2] where Ni is substantially less prone to oxidation than Al. In the iron aluminides both elements have a high affinity for oxygen, which complicates the understanding of the oxidation process as a function of the thermodynamic parameters. It is a challenge to contemporary surface science to understand and control on a microscopic scale such an oxidation process.

It is well established that binary alloys show preferential surface segregation of one of their constituents,[3] thereby altering physical properties in the subsurface region. The clean $Fe_3Al(110)$ surface exhibits an order-disorder phase transition around 820 K that in the subsurface region shows a temperature dependence which differs substantially from the bulk.[4,5] This can be understood from the segregation of Al to the surface.[6] The resulting subsurface compositional changes will lead to modifications in the atomic ordering of binary alloys such as the iron aluminides. It may be expected that the presence of oxygen has a large effect on the surface segregation. Such processes are known to be detrimental to stainless steels, where chromium segregates preferentially, thereby triggering pitting corrosion[7] and crack formation.[8]

This work is intended to obtain a better understanding of the oxidation behavior of a binary alloy which has a large potential as a structural material. Furthermore, it is aimed at obtaining a better general understanding of the segregation and subsequent ordering processes in the subsurface region of binary alloys under oxidizing conditions. To tackle this difficult problem we use surface x-ray diffraction in combination with Auger electron spectroscopy (AES). While the former technique is ideally suited to follow the order in the (sub)surface region, the latter allows one to obtain a view of the chemical composition of the topmost layers. As a starting point for future investigations, the present work focuses on the clean $Fe_3Al(110)$ surface and on its oxidation at $10^{-6}$ mbar $O_2$ and 573 K.[4]

In the following paragraphs the atomic structure of bulk $Fe_3Al$ and the resulting scattering pattern are introduced, after which the details of the experiments are given. Finally the experimental results are discussed and conclusions are drawn.

## II. BULK $Fe_3Al$ AND ITS (110) FACE

The part of the Fe-Al phase diagram of interest to the present study[9] shows three phases (A2, B2, and $D0_3$), which differ in the decoration of atoms over the underlying fundamental body-centered-cubic (bcc) lattice (Fig. 1). To describe the structures it is useful to introduce three different sublattices giving rise to the crystallographic sites $\alpha$, $\beta$, and $\gamma$; see Fig. 1. The superstructure Bragg reflections arising from the $D0_3$ phase, first described by Bradley and Jay,[10] are a direct measure for the ordering of Fe and Al over the $\beta$ and $\gamma$ sites.

Crystal truncation rods (CTRs) (Refs. 11 and 12) arising due to the abrupt (110) termination of a $D0_3$ crystal connect Bragg peaks *hkl* that probe different types of ordering. Here, the surface coordinates are defined as shown in Fig. 1 with $a=5.79$ Å, and $b=c=4.09$ Å. This leads to CTRs with $h=2n+1$, where $n=0,1,2,3\ldots$, originating only from the superlattice peaks of the $D0_3$ ordering. In the same way the (110) surface distinguishes between CTRs probing the order of the underlying A2-type fundamental bcc lattice ($h+2k=4n$) and the B2-type decoration of atoms over the bcc lattice points ($h+2k=4n+2$). This is seen by evaluating the structure factor, $F$, of the Bragg peaks along different types of CTRs;

$$F_{h+2k=4n} = (2f_\alpha + f_\beta + f_\gamma)(e^{i\pi k} + e^{i\pi l}),$$

$$F_{h+2k=4n+2} = (2f_\alpha - f_\beta - f_\gamma)(e^{i\pi k} + e^{i\pi l}),$$

$$F_{h=2n+1} = (f_\beta - f_\gamma)e^{i(\pi/2)h}(e^{i\pi k} - e^{i\pi l}), \quad (1)$$

with the scattering contribution of each site given by

 

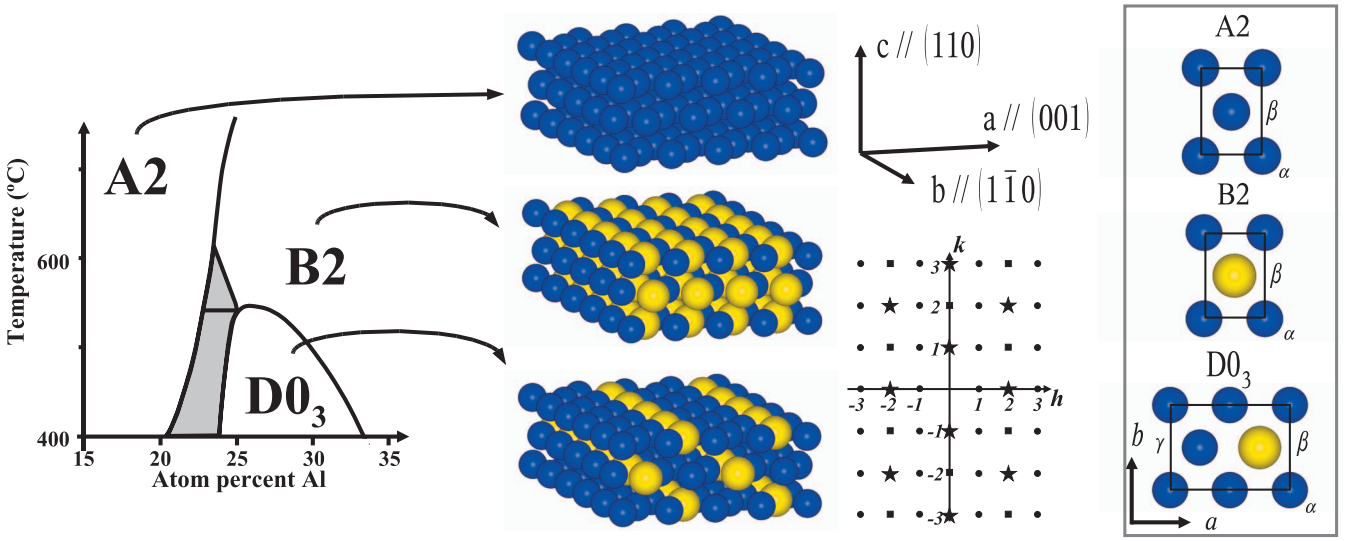


FIG. 1. (Color) Part of the Fe-Al phase diagram (Ref. 9) showing the three phases A2, B2 and $D0_3$. The gray area indicates phase separation. The bulk terminated (110) surfaces of each of the three phases of $Fe_xAl_{1-x}$ are represented as crystal slabs, with ideal compositions of Al (yellow) and Fe (blue), i.e., $x=1$ (A2, top), $x=\frac{1}{2}$ (B2, middle) and $x=\frac{3}{4}$ ($D0_3$, bottom). The panel on the right-hand side shows the topmost atoms of the (110) surface unit cells in their *ab* planes and the corresponding $\alpha$, $\beta$, and $\gamma$ sites. The definition of the surface unit cell with respect to the underlying elementary bcc lattice is given in the middle upper part. Underneath the *hk* plane in reciprocal space at $l=0$ is drawn, showing the Bragg reflections probing A2 (■), B2 (⋆), and $D0_3$-type (●) order.

$$f_j = \theta_j^{\mathrm{Fe}} f_{\mathrm{Fe}} + \theta_j^{\mathrm{Al}} f_{\mathrm{Al}}, \quad \text{for } j = \alpha, \beta, \gamma, \tag{2}$$

where $f_{\mathrm{Fe}}$ and $f_{\mathrm{Al}}$ are the atomic scattering factors for Fe and Al, respectively. The occupancy of site $j$ is given by $\theta_j^p$, with $p$=Fe or Al.

In the bulk it is not expected that vacancies form the majority defect. Slight changes in the stoichiometry compared to the ideal $D0_3$ composition $Fe_3Al$ result in antisite atoms,[13] i.e., the energy cost of a "wrong" atom on the $\beta$ or $\gamma$ site is almost zero.[13,14] The samples used in the present work are slightly rich in Al, because this assures that upon heating one stays away from the phase-separation region; see Fig. 1. If one assumes that the excess of Al sits only on $\gamma$ sites and that there is no vacancy formation, the scattering contributions for each site as given by Eq. (2) become $f_\alpha = f_{\mathrm{Fe}}$, $f_\beta = f_{\mathrm{Al}}$, and $f_\gamma = (1-\epsilon) f_{\mathrm{Fe}} + \epsilon f_{\mathrm{Al}}$, with $\epsilon < 1$ an arbitrary number. Using these scattering contributions to compare structure factors of samples rich in Al ($F^{\epsilon}_{hkl}$) and of ideal $D0_3$ stoichiometry ($F^{0}_{hkl}$), one obtains

$$F^{\epsilon}_{h+2k=4n} = \epsilon(f_{\mathrm{Fe}} - f_{\mathrm{Al}})(e^{i\pi k} + e^{i\pi l}) + F^{0}_{h+2k=4n},$$

$$F^{\epsilon}_{h+2k=4n+2} = (1+\epsilon) F^{0}_{h+2k=4n+2},$$

$$F^{\epsilon}_{h=2n+1} = (1-\epsilon) F^{0}_{h=2n+1}. \tag{3}$$

One can now introduce order parameters $m_{D0_3} = (1-\epsilon)$ and $m_{B2} = \frac{1}{2}(1+\epsilon)$, such that the different kinds of Bragg peaks scale quadratically with them.[15] The different kinds of CTRs behave differently upon the Al enrichment. Whereas the $D0_3$-type CTR decreases, the B2-type CTR increases due to the fact that one is closer to the ideal B2 composition FeAl and away from the ideal $D0_3$ one. The CTR probing the A2-type order is merely changed by the difference in total composition and will therefore never vanish, irrespective of the composition. These details are important in an atomic surface structure refinement, since they systematically introduce corrections in order to get all the computed CTRs on the right scale.

## III. EXPERIMENT

Single crystals of nominal composition $Fe_{0.72}Al_{0.28}$ were grown, cut, and polished in-house at the Max Planck Institute for Metals Research (MPI-MF) in Stuttgart, Germany. High-energy x-ray diffraction of the final platelike samples showed excellent crystallinity in the bulk, with typical Bragg reflection rocking curve widths better than 0.01°.

*In situ* surface x-ray diffraction (SXRD) experiments were performed using a portable ultrahigh vacuum (UHV) oxidation chamber at beamline ID03 (Ref. 16) of the European Synchrotron Radiation Facility (ESRF) in Grenoble, France, and at the MPI-MF beamline[17] at the Ångström-Quelle Karlsruhe (ANKA), Germany. In all experiments, a monochromatic x-ray beam ($\Delta E/E \simeq 10^{-4}$) with photon energy $E$ around 10 keV was used.

For the experiments two different samples, named 1 and 2 hereafter, were used. Sample 1 was measured at ID03 and sample 2 at ANKA. Due to the difference in photon flux at the two beamlines (approximately 3 orders of magnitude more at ID03 than at the ANKA beamline), only for sample 1 all types of rods could be measured. The signal on the $D0_3$ superstructure CTRs ($h=2n+1$) during the measurements on sample 2 was too weak.

Clean and well-ordered surfaces, as confirmed by (1 × 1) low-energy electron diffraction (LEED) patterns, were obtained by repeated cycles of annealing and sputtering with $Ar^+$ ions (energy $E=1.5$ keV, sputter current 10 $\mu$A cm$^{-2}$).

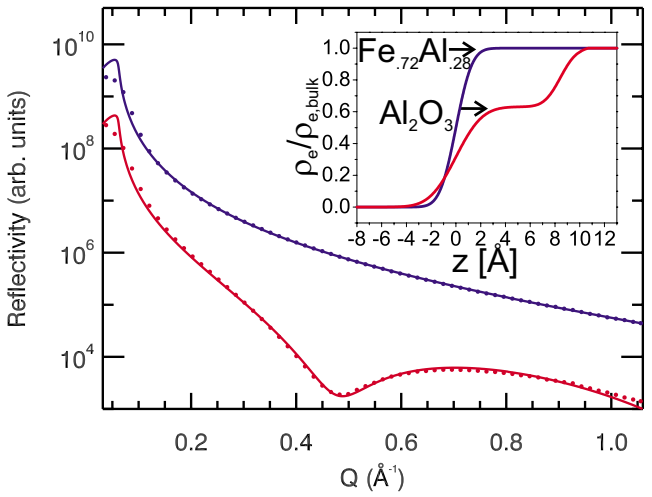


FIG. 2. (Color online) X-ray reflectivity curves obtained from the clean (blue, upper) and oxidized (red, lower) surface; the curves are displaced for clarity. Shown are the experimental data (points) and fits (solid lines) using the Parratt formalism (Ref. 19), the results of which are given in Table I. The inset shows the resulting electron density ($\rho_e$) profiles for the clean (blue, upper) and oxidized (red, lower) surfaces as a function of the $z$ direction along the surface normal.

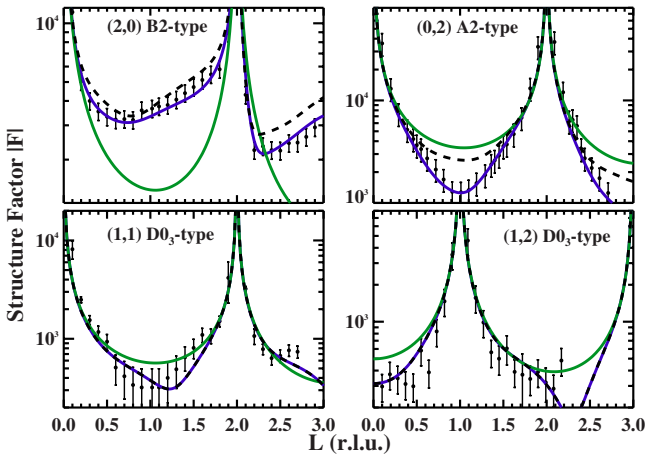


FIG. 3. (Color online) Experimental CTR data (points) of the clean surface and the results of different structural models (lines). Shown are the following: best fit (blue solid line, darker), bulk terminated (green solid line, lighter), and a calculation for a structure as in the best fit, only without any vacancies (black dashed line). Note that for the $D0_3$-type CTRs the best fit model with and without vacancies give the same curve. This is because most of the vacancies appear in the topmost layer, which has a B2-inplane symmetry thereby not contributing to the $D0_3$-type CTRs.

After the final high-temperature anneal step at 1173 K, special care was taken to not cool the samples too quickly through the B2-$D0_3$ phase transition at 820 K. This would cause many $D0_3$ antiphase domains[18] and therefore broadened superstructure CTRs, resulting in poor signal-to-noise ratios.

## IV. RESULTS

### A. Atomic structure of the clean surface

After the cleaning procedure as described in Sec. III, a typical x-ray reflectivity curve, shown in Fig. 2, exhibits a Fresnel-type shape which indicates that there is a near-perfect vacuum-crystal interface. The results of fitting a density profile to the reflectivity data shown in Fig. 2 using the Parratt formalism[19] render a smooth $Fe_3Al$ surface. The results are listed in Table I.

The crystallographic surface diffraction data, obtained by taking rocking scans at each point along the CTRs, were integrated and corrected in a standard way.[20] The program ROD (Ref. 21) was used to fit different structure models to the experimental structure factors, which are shown in Fig. 3.

TABLE I. Results of the x-ray reflectivity measurements of the clean and oxidized surfaces. The root-mean-square roughness ($\sigma$) for the interfaces as well as the oxide thickness ($t$) are shown.

| Parameter | Clean | Oxidized |
|---|---|---|
| $\sigma_{Fe_3Al}$ (Å) | 1.0(8) | 1.0(5) |
| $\sigma_{ox}$ (Å) | | 1.7(6) |
| $t_{ox}$ (Å) | | 8.4(3) |

The scattering from the bulk is calculated by using Eqs. (1) and (3) with $\epsilon$=0.12, which follows from the Al-enriched nominal composition $Fe_{3-\epsilon}Al_{1+\epsilon}$. The Debye-Waller parameters of all atoms are kept at bulk values,[22] with $B_{Fe}$=0.345, and $B_{Al}$=0.45.

When comparing the experimental data with the CTRs calculated for a bulk terminated crystal, one sees that the (1,1), (1,2), and (0,2) rods are fairly well reproduced. However, the (2,0) rod is much higher in intensity than the simulation for bulk termination. This rules out that roughness alone can explain the observed rod profiles, since surface roughness would lower all rods in between the Bragg peaks. Qualitatively, from the differences between the bulk termination simulation and the experimental data one can directly conclude that the surface orders in a different symmetry compared to the underlying bulk. Since the (2,0) rod probes the B2-type order in the surface region, one can conclude that in the surface the $\beta$ and $\gamma$ sites are crystallographically equivalent. This leads to additional scattering from these layer(s) contributing to the (2,0) rod, without affecting the (1,1) and (1,2) rods.

Having identified that the largest discrepancy between bulk termination and a B2-like overlayer appears on the (2,0) rod, one sees that there is a lot of extra intensity between the Bragg peaks along the (2,0) rod. The parameters that are responsible for this feature are the rumpling of the atoms in the topmost layer and their occupancies. Fitting these together with structural relaxations and minor disorder in the second and third layer leads to the best fit results presented in Table II.

In the refinement procedure for sample 2 fewer parameters are used, because the total data set is smaller than for sample 1 as discussed in Sec. III. Nevertheless, the results for both samples 1 and 2 agree very well. This is because the

TABLE II. Results of the structural refinement procedures listing displacements $\Delta z_p$ and occupancies $\theta_p$ with $p=1,2$ for samples 1 and 2. Given are the displacements from the ideal fractional coordinates as occurring in the bulk, in which the spacing between consecutive atomic layers is $0.5c=2.045$ Å. The best fits of the CTRs of sample 1 are shown in Fig. 3. The atoms are labeled as Elno.$^j$, where the element El=Fe, Al (or vacancy □), then the number (no.) of the layer, where 1 is the surface and $j=\alpha,\beta,\gamma$, indicates the particular lattice site.

| | Sample 1 | | Sample 2 | |
|---|---|---|---|---|
| Atom | $\theta_1$ (–) | $\Delta z_1$ (–) | $\theta_2$ (–) | $\Delta z_2$ (–) |
| $Fe1^{\alpha}$ | 0.79(3) | 0.025(3) | 0.83(2) | 0.010(5) |
| $\square 1^{\alpha}$ | 0.21(3) | | 0.17(2) | |
| $Al1^{\beta,\gamma}$ | 0.65(4) | –0.017(6) | 0.96(3) | –0.02(1) |
| $\square 1^{\beta,\gamma}$ | 0.35(4) | | 0.04(3) | |
| $Fe2^{\alpha}$ | 0.96(2) | 0.003(2) | 1.00(1) | –0.004(3) |
| $\square 2^{\alpha}$ | 0.04(2) | | 0.00 | |
| $Al2^{\beta}$ | 1.00 | 0.011(5) | 1.00 | –0.010(5) |
| $Fe2^{\gamma}$ | 0.71(2) | 0.003(3) | 0.88 | 0.00 |
| $Al2^{\gamma}$ | 0.30 | 0.003(3) | 0.12 | 0.00 |
| $Fe3^{\alpha}$ | 1.00 | 0.00 | 1.00 | 0.00 |
| $Al3^{\beta}$ | 1.00 | –0.006(3) | 1.00 | 0.00 |
| $Fe3^{\gamma}$ | 0.88 | 0.002(2) | 0.88 | 0.00 |
| $Al3^{\gamma}$ | 0.12 | 0.002(2) | 0.12 | 0.00 |

relaxations in deeper layers, which exhibit $D0_3$ symmetry, are negligibly small. The most important features in the data arise from the topmost layer, which shows in-plane B2-type order.

### B. Atomic structure of the oxidized surface

After exposing the clean sample to $10^{-6}$ mbar of molecular oxygen for 30 min at 573 K, the x-ray reflectivity curve (see Fig. 2) shows a well-defined dip around $Q=0.5$ Å$^{-1}$ indicating that an oxide layer has formed on the surface. The best fit is obtained by assuming an electron density of bulk $Al_2O_3$ for the thin oxide layer and smooth interfaces to the underlying substrate and the vacuum above, as listed in Table I. This implies that there is no formation of iron oxide, a finding which will be discussed in more detail further on.

After the oxidation, the intensity along the (2,0), (1,1), and (1,2) rods has almost completely vanished. A typical rocking scan at a point along the (2,0) rod before and after oxidation is shown in Fig. 4(b). The (0,2) rod, shown in Fig. 4(a), became most significantly weaker halfway the Bragg peaks. None of the Bragg peaks' intensity changed, which means that only in the near-surface region drastic structural changes have occurred.

The different experimental observations after oxidation are summarized as follows: a thin smooth aluminum-oxide layer is formed on top of a substrate that in the near-surface region has neither B2 nor $D0_3$ order. This means that the lattice itself, as defined by the A2 bcc structure, is not destroyed, neither have the interfaces become (much) rougher.

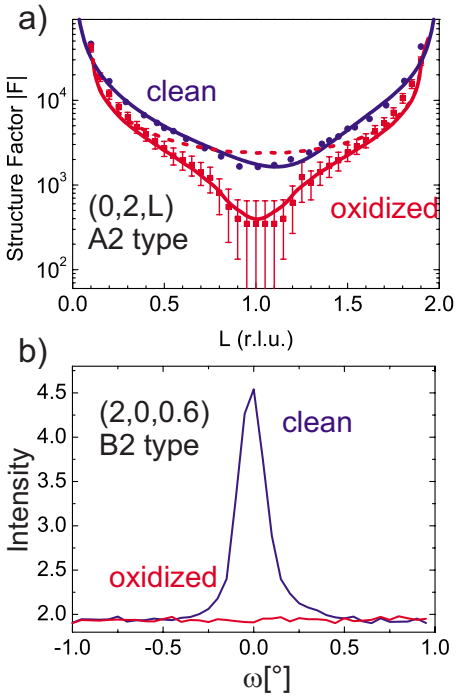


FIG. 4. (Color online) (Top) Experimental (0,2) CTR before (blue, upper) and after (red, lower) the oxidation procedure as described in the text. The simulation (red solid line) is performed for a $D0_3$ bulk crystal of which the topmost layers gradually change their composition as described in the text and as schematically shown in Fig. 5. Also shown is the simulation (dashed red) for the case that the interface between the oxide and the substrate would be perfectly sharp, i.e., no clustering of Fe would take place. (Bottom) The rocking scan at the point (2,0,0.6) of the clean (blue) and oxidized (red) surface. Clearly, for this rod the intensity disappears completely upon oxidation.

These findings raise the following questions: (i) Up to which depth is the superlattice in the subsurface region disordered? (ii) Is the disorder due to a change in the composition? These questions will be addressed hereafter by further data analysis and simulation.

A rough estimate of the thickness over which the structure is disordered can be obtained by calculating from how many substrate layers Al is needed to form the 8.4 Å thin oxide. Taking the electron density of bulk $Al_2O_3$ results in 4 unit-cell layers of $Fe_{0.72}Al_{0.28}$ to be completely Al depleted. This is reduced by half a unit-cell layer when the composition of the topmost atomic layer of the surface is FeAl, which follows from the results for the clean surface presented in Sec. IV A.

In general, diminishing CTR signals are caused by an average decrease in electron density in the surface region. This can be the result of either compositional changes or an increase in surface roughness. A drastic increase in surface roughness can be ruled out on the basis of the results of the x-ray reflectivity measurements shown in Fig. 2 and Table I. The oxide layer has a well-defined thickness and shows smooth interfaces to the underlying substrate and to the vacuum. Therefore, another explanation is needed in which the CTRs originating from the B2 and $D0_3$ superlattices are

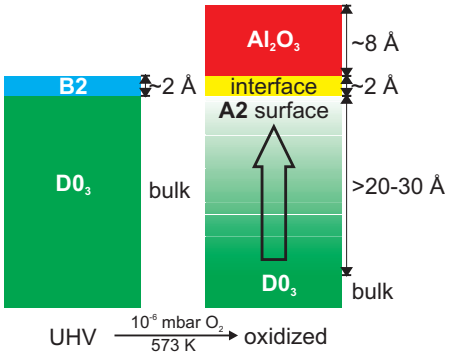


FIG. 5. (Color) Schematic representation of the clean (left) and oxidized (right) surface. The clean surface, which was investigated in UHV, shows a topmost atomic layer having B2 symmetry on a $D0_3$ bulk crystal. The oxidized surface shows a gradually changing superlattice order in the subsurface region. The order starts with $D0_3$ in the bulk and changes to A2 at the interface with the oxide. The interface layer has A2 symmetry but a reduced average density which is the result of complete Al depletion in the topmost atomic layer which before oxidation consisted of $Fe_{0.5}Al_{0.5}$.

suppressed, but not the CTR probing the fundamental bcc lattice. A solution can be given by the $D0_3$ and B2 order parameters decreasing gradually from the bulk toward the surface. The exact profile of such a transition cannot be determined from the present data, simply because the signals vanished. Nevertheless, and without losing generality, one can investigate the influence of such a disordering process on the CTR signals. The average scattering of each unit-cell layer in the subsurface region can be viewed as a weighted average of two contributions consisting of a $D0_3$ (and with that also B2) and an A2 part. Here, the weighting is performed by using the so-called $\beta$-roughness model,[23] since it gives a simple and exact solution by

$$F = \underbrace{F_{\mathrm{CTR}} + \sum_{j=1}^{n} \beta^j F_{\mathrm{bulk}} e^{i2\pi lj}}_{\mathrm{D0_3,B2}} + \underbrace{\sum_{j=1}^{n} (1-\beta^j) F_{\mathrm{surf}} e^{i2\pi lj} + \theta F_{\mathrm{interface}}}_{\mathrm{A2}}, \tag{4}$$

with $F_{\mathrm{CTR}}$ as the CTR scattering, $F_{\mathrm{bulk}}$ as the scattering from a $D0_3$ bulk unit cell, $F_{\mathrm{surf}}$ as the scattering from an A2 surface unit cell, and $\beta^j$ as the occupation in the $j$th layer above the bulk (see Fig. 5 for a schematic view). The A2 structure is calculated by assuming completely Al-depleted unit cells, resulting in the $\alpha$, $\beta$, and $\gamma$ sites being occupied by 0.72 Fe atoms. The oxide film has a very poor crystallinity and does not therefore contribute to CTR scattering with in-plane momentum transfer. The interface between the oxide and the subsurface region is not uniform, but shows atomic disorder or roughness. This is modeled by assuming an interface layer of reduced density, having a coverage $\theta$ and scattering contribution $F_{\mathrm{interface}}$ with A2 symmetry. This describes the scattering for a layer which consists either of a mix of A2 and oxide material or an A2 layer containing many vacancies. The first two terms on the right-hand side of Eq. (4) involve bulk scattering and therefore have a $D0_3$ (and also B2) symmetry. These two terms together render CTRs of which the intensity is reduced between the Bragg peaks as in the case of roughness. The next two terms in Eq. (4) involve scattering by materials having A2 symmetry. They do not contribute to the B2 and $D0_3$ rods, thereby not changing the shape as established by the first two terms. However, the contribution to the A2 rods is such that their shape does not change too much from having a well-defined smooth surface region. The characteristic shape of the (0,2) rod shows a strong dip halfway the Bragg peaks, which is well reproduced by the interface layer of reduced density. Figure 4 shows a simulation of the previously described model as parametrized by Eq. (4).[24] With a gradually changing order parameter not each unit-cell layer is completely Al depleted. The previously estimated depth up to which the disorder takes place ($N_{\mathrm{tot}}$=3.5–4) will therefore be enlarged depending on the disordering profile that is used. For the $\beta$-roughness model that is used here, the depth up to which the disorder takes place ($n$) is closely related to the parameter $\beta$ by $\frac{\beta-\beta^{n+1}}{1-\beta}=N_{\mathrm{tot}}$. The simulations shown in Fig. 4 are therefore performed with $\beta$=0.85 and $n$=8. These values lead to a decrease of at least 1 order of magnitude on $F$ of the B2 and $D0_3$ rods (2 orders of magnitude in intensity), which complies with the detection limit in the experiments. To show the effect of the interface structure between the oxide and the substrate, the (0,2) rod is simulated as well when assuming that an interface with reduced density is absent ($\theta$=0). In that case the characteristic dip is not present and the intensity is close to the CTR of the clean surface.

### C. Chemical composition of the oxide layer

The chemical composition of the topmost surface layers is studied by AES. Figure 6 shows spectra for the clean surface and after oxidation at $10^{-6}$ mbar at 573 K for 30 min. Surface cleanliness was pursued in a standard way of sputtering and annealing. However, as shown in Fig. 6 even after many cycles of prolonged sputtering and annealing (up to 2 h and 1500 K per cycle), still a small oxygen signal remains present. Although some remains of oxide patches cannot be excluded, most likely for a large part the remaining oxygen signal is due to the adsorption of CO, which at the UHV base pressure of approximately $5\times10^{-10}$ mbar is still present in small amounts. This also correlates with a tiny carbon signal in the AES spectrum (not shown) that is present after cleaning the surface. It is known that CO absorbs molecularly at room temperature on $Fe_{0.6}Al_{0.4}(110)$ at exposures even below 1 L,[25] which underlines the above-mentioned hypothesis. Nevertheless, all the results presented here are not very sensitive to such a minor contamination, in particular since the coverage is expected to be very small.

The low-energy part of the AES spectrum lends itself for the identification of oxides on the surface. Bonding of Fe or Al with oxygen leads to a chemically shifted AES transition,[26,27] which has shown to be an adequate tool for

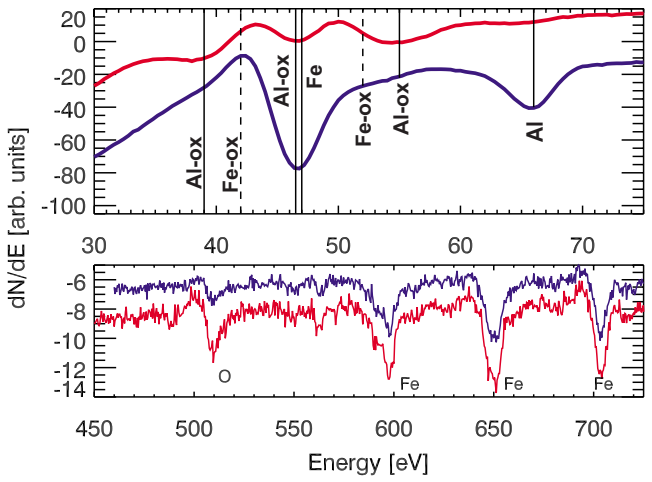


FIG. 6. (Color online) AES spectra of the $Fe_3Al(110)$ surface. The top graph shows the low-energy part for the clean (blue, lower) and oxidized (red, upper) surface; the curves are displaced for clarity. The vertical lines indicate the following elements: metallic Al (66 eV), metallic Fe (47 eV), oxidized Al (39, 46.5, and 55 eV) and oxidized Fe (42 and 52 eV). After oxidation, there are no signs of the formation of iron oxides, as indicated by the dashed vertical lines. The bottom part shows the spectra in the energy range where the oxygen (510 eV) and Fe (598, 651 and 703 eV) signals are visible; clean (blue, upper) and oxidized (red, lower).

the identification of oxide formation on Fe(110) (Ref. 28) and NiAl(110).[29] Figure 6 clearly shows that the clean surface shows hardly any traces of oxides, whereas the oxidized surface shows mostly aluminum oxide and no iron oxide.

## V. DISCUSSION

### A. Clean surface

The results from the SXRD measurements on the clean surface clearly demonstrate that the topmost atomic layer has an in-plane B2 symmetry. This implies preferential surface segregation of Al, thereby destroying the $D0_3$ order in this layer. A related mechanism has been found for similar systems, such as $Ni_{0.9}Al_{0.1}(110)$. In this fcc compound the topmost layer exhibits the ordered $L1_2$ structure on top of an A1 bulk due to aluminum segregation, resulting in a composition of $Ni_{0.75}Al_{0.25}$.[30] A low-energy ion scattering (LEIS) study of the $Fe_3Al(110)$ surface showed that at room temperature the topmost layer has the composition FeAl.[6] The present results corroborate the idea of Al enrichment at the surface. However, whereas the Fe concentration for samples 1 and 2 are similar, the Al content seems not to be unambiguously determined. This could be for the following reasons. First, this could be due to a difference in surface preparation, during which preferential sputtering of Al takes place. During the subsequent annealing procedure Al may segregate again, but at temperatures higher than approximately 1150 K, Al starts to evaporate from the surface.[31] Second, the scattering contribution of Al being relatively low makes it difficult to unequivocally obtain unrestrained fit parameters. Last, there is a large correlation between the fit parameters, especially between the occupation and displacements of the topmost $\beta$ and $\gamma$ sites, the scale factor, and the surface roughness. In order to keep the number of parameters as low as possible, surface roughness was not explicitly put in the models. Therefore, the occupancies of the atoms should not be taken as a measure for the vacancies, but more as the total influence of several factors playing a role at different length scales. These include vacancies, atomic roughness, and macroscopic roughness (curvature of the surface), all of which for samples 1 and 2 could have been different. However, since the presently used diffraction method is an excellent probe for the atomic order and symmetry, the model in which a B2-type surface layer terminates a $D0_3$ crystal describes all the features of the data obtained for both samples very well.

For FeAl, which in the bulk already adopts the B2 structure, it is reported that the segregation of Al leads to a composition $FeAl_y$ (with $y>1$) of the clean (110) surface.[31,32] The LEED patterns for this surface never show a $(1\times1)$ structure. For the composition $FeAl_2$ of the topmost layer there is the formation of an incommensurate $(2\times1)$ reconstruction,[33] whereas for other compositions the surface layers are disordered in at least one direction. Apparently, the bulk stoichiometry close to $Fe_3Al$ leads after segregation to exactly the right amount of Al to form a well-ordered surface structure which is commensurate with the underlying $D0_3$ bulk.

The results from the surface structure refinement indicate that for both samples the topmost layer shows a corrugation where the Fe atoms are pulled out of the surface. Within two times the estimated standard deviation (e.s.d.) the values obtained for both samples are identical. In general one would expect the larger of the two atoms, in this case Al, being pulled out of the surface, as observed for NiAl(110),[34,35] $Ni_3Al(110)$,[36] and CoAl(110).[37] Although these examples show the expected general behavior, the presence of magnetism might give just the opposite.[38] A surface leads to a narrowing of the *d* band, which in turn enlarges the surface density of states.[39] Hereby the magnetic moment at the surface is expected to be enhanced. The system can reduce the gain in magnetic energy by a structural relaxation whereby the magnetic element is pulled out of the surface. Since iron has a substantial magnetic moment (2.2 $\mu_B$ for pure Fe), the previously described effect could be responsible for the observed surface corrugation in $Fe_3Al$.

### B. Oxidized surface

A simple structural model that complies with all the experimental observations of the oxidized samples is shown in Fig. 5. The main feature consists of a gradually changing order, going from $D0_3$ (and B2) in the bulk toward A2 at the interface between the crystal and the oxide layer. Furthermore, the interface layer between substrate and oxide shows a largely reduced density which can be interpreted as atomic roughness. Since this interface emerges from the B2 layer that is observed for the clean surface, it is expected that after all the Al has been taken out the average density corresponds to half a monolayer of iron. Reverting to the two questions raised in Sec. IV B: (i) From the thickness of the oxide layer one can obtain a rough estimate of the thickness over which

the subsurface region is Al depleted. To get a more accurate result, the depletion profile should be known. (ii) Pinpointing the exact composition is difficult, since the difference in x-ray scattering power between bulk and Al-depleted $Fe_3Al$ is only 15%. This is illustrated by the simulations in Fig. 4, which show that the calculated CTRs for the clean surface (close to bulk termination) and for the Al-depleted subsurface region are almost identical. A more detailed understanding by modeling of both issues is further hampered since only a limited amount of data of the oxidized surface is available, simply because the signals vanished.

It is known that the mechanical properties of alloys of Fe and Al depend strongly on the stoichiometry. With increasing Al content, room-temperature ductility and high-temperature strength become worse.[1] Therefore, it is expected that the mechanical properties in the subsurface region change after oxidation. In the case that the subsurface region would consist of pure iron, it would be expected to be more ductile.[40] However, it is not expected that the subsurface region has a structure similar to bulk iron, since after oxidation either Al segregates into this region or many vacancies remain present. In the latter case, it would be expected that an extremely brittle structure would arise, since many bonds are absent. Even if clustering of Fe would occur, the grain structure would be such that individual grains could move easily since they have a lot of free space around them. Unfortunately, there is not much known about the ternary phase diagram of Fe, Al, and vacancies.

Depletion zones can cause severe local chemical changes which can be detrimental to structural materials. For stainless steel, where chromium oxide forms the protective layer, it is known that chromium depletion plays an important role for the corrosion properties. Local chemical changes around MnS inclusions caused by chromium depletion result in an extremely aggressive solution which accelerates pitting corrosion.[7] Chromium depletion, triggered by chromium carbide precipitation, at grain boundaries in stainless steel is one of the major reasons for intergranular corrosion and is a precursor to crack development.[8,41] It is to be expected that also in the case of the iron aluminides these processes play an important role.

In comparison to the oxidation of related compounds, there are significant differences. In the case of NiAl(110), the near-surface region does not lose its B2 structure upon oxidation at the same conditions.[35] This can be understood by NiAl being strongly ordering, in contrast to $Fe_3Al$.

It has been reported that the oxidation of the FeAl(110) surface at elevated temperatures results in the formation of an ordered oxide film,[42] of which the LEED pattern bears much resemblance with the one of the oxidized NiAl(110) surface.[2] Spectroscopic measurements indicate that this layer consists of aluminum oxide.[32,42,43] However, for different conditions, leading to higher oxidation rates, also the formation of iron oxides has been observed.[42,44] Our results, indicating only the formation of aluminum oxide, agree with the aforementioned studies.

## VI. CONCLUSIONS

The clean $Fe_3Al(110)$ surface comprises a topmost atomic layer with in-plane B2-type order on a $D0_3$ ordered bulk crystal. Upon oxidation for 30 min at $10^{-6}$ mbar of molecular oxygen at a temperature of 573 K, the $D0_3$ and B2 orders disappear completely in the subsurface region. Assuming a $\beta$-roughness-like profile for the disorder, whereby the $D0_3$ and B2 order parameters diminish from the bulk to the surface, results in a depth of 2–3 nm for the disordered region. At the same time an 8.4 Å thin smooth oxide layer is formed on the surface. This means that the oxidation-induced disorder in the subsurface region affects only the decoration of Fe, Al, and vacancies over the underlying bcc lattice, and not its crystallinity. The analysis of the AES spectra for these oxidation conditions shows only the formation of aluminum oxide. These findings can be understood by considering preferential surface segregation and selective oxidation of Al. The clean surface is Al enriched, while after oxidation the Al-depleted subsurface region lacks the Al for long-range superlattice order as it appears in the bulk.

The results of the present study are of importance to the application of iron aluminides under realistic conditions. It is indispensable that a protective oxide scale is formed on the surfaces of such materials to protect them from aggressive environments. The fact that there are drastic compositional changes in an extended subsurface region indicates that the process is not only limited to the very surface. This can have consequences for the processing and integration of iron aluminides in devices, since the physical properties, such as ductility and strength, depend on the composition. However, at the time there is little known about the mechanical properties of these alloys in the case that they contain many vacancies. Nevertheless, it may be expected that the oxidation process renders these materials more brittle and vulnerable to aggressive environments.

## ACKNOWLEDGMENTS

The authors are greatly indebted to R. Henes, I. Sorger and in particular to A. Weisshardt of the MPI for Metals Research for their instrumental help with the sample growth and preparation. H. Reichert, A. Díaz-Ortiz, and M. Fähnle are acknowledged for helpful discussions. Furthermore we would like to thank R. Weigel of the MPI-MF and the ID03 staff at the ESRF for help during the experiments.

*vonk@mf.mpg.de; http://www.mf.mpg.de

[1] C. G. McKamey, J. H. DeVan, P. F. Tortorelli, and V. K. Sikka, J. Mater. Res. **6**, 1779 (1991).
[2] J. Libuda, F. Winkelmann, M. Baumer, H. J. Freund, T. Bertrams, H. Neddermeyer, and K. Muller, Surf. Sci. **318**, 61 (1994).
[3] S. Müller, J. Phys.: Condens. Matter **15**, R1429 (2003).
[4] L. Mailänder, H. Dosch, J. Peisl, and R. L. Johnson, Phys. Rev. Lett. **64**, 2527 (1990).
[5] H. Dosch, L. Mailänder, R. L. Johnson, and J. Peisl, Surf. Sci. **279**, 367 (1992).
[6] D. Voges, E. Taglauer, H. Dosch, and J. Peisl, Surf. Sci. **269-270**, 1142 (1992).
[7] M. P. Ryan, D. E. Williams, R. J. Chater, B. M. Hutton, and D. S. McPhail, Nature (London) **415**, 770 (2002).
[8] M. Shimada, H. Kokawa, Z. J. Wang, Y. S. Sato, and I. Karibe, Acta Mater. **50**, 2331 (2002).
[9] F. Stein and M. Palm, Int. J. Mater. Res. **98**, 580 (2007).
[10] J. A. Bradley and A. H. Jay, Proc. R. Soc. London, Ser. A **136**, 210 (1932).
[11] R. Feidenhans'l, Surf. Sci. Rep. **10**, 105 (1989).
[12] I. K. Robinson, *Handbook on Synchrotron Radiation* (North-Holland, Amsterdam, 1991), Vol. 3, Chap. 7, pp. 221–266.
[13] M. Fähnle and L. Schimmele, Z. Metallkd. **95**, 864 (2004).
[14] G. Bester, B. Meyer, and M. Fähnle, Phys. Rev. B **60**, 14492 (1999).
[15] The order parameters $m=m(\epsilon,T)$ are a function of the composition (described by $\epsilon$) and temperature ($T$). Here the temperature-independent part is described.
[16] S. Ferrer and F. Comin, Rev. Sci. Instrum. **66**, 1674 (1995).
[17] A. Stierle, A. Steinhäuser, A. Rühm, F. U. Renner, R. Weigel, N. Kasper, and H. Dosch, Rev. Sci. Instrum. **75**, 5302 (2004).
[18] M. Marcinkowski and N. Brown, J. Appl. Phys. **33**, 537 (1962).
[19] L. G. Parratt, Phys. Rev. **95**, 359 (1954).
[20] E. Vlieg, J. Appl. Crystallogr. **30**, 532 (1997).
[21] E. Vlieg, J. Appl. Crystallogr. **33**, 401 (2000).
[22] Y. Komura, Y. Tomiie, and R. Nathans, Phys. Rev. Lett. **3**, 268 (1959).
[23] I. K. Robinson, Phys. Rev. B **33**, 3830 (1986).
[24] Equation (4) contains a sharp transition between the bulk and the distorted surface region and a finite sum over distorted layers. These two features lead to finite thickness oscillations in the rod profiles, which are experimentally not observed. Most likely, the interface between the bulk and the distorted region is not atomically sharp. Consequently, for the rod calculation the ensemble average over many different thicknesses should be taken. To account for this effect, the simulation includes a convolution with a top-hat function of width $\Delta l=0.1$.
[25] N. R. Gleason and D. R. Strongin, Surf. Sci. **295**, 306 (1993).
[26] D. T. Quinto and W. D. Robertson, Surf. Sci. **27**, 645 (1971).
[27] M. Suleman and E. B. Pattinson, Surf. Sci. **35**, 75 (1973).
[28] V. S. Smentkowski and J. J. T. Yates, Surf. Sci. **232**, 113 (1990).
[29] H. Isern and G. R. Castro, Surf. Sci. **211-212**, 865 (1989).
[30] R. Drautz, H. Reichert, M. Fähnle, H. Dosch, and J. M. Sanchez, Phys. Rev. Lett. **87**, 236102 (2001).
[31] H. Graupner, L. Hammer, K. Muller, and D. M. Zehner, Surf. Sci. **322**, 103 (1995).
[32] O. Kizilkaya, D. A. Hite, D. M. Zehner, and P. T. Sprunger, Surf. Sci. **529**, 223 (2003).
[33] A. Baddorf and S. Chandavarkar, Physica B (Amsterdam) **221**, 141 (1996).
[34] H. L. Davis and J. R. Noonan, Phys. Rev. Lett. **54**, 566 (1985).
[35] A. Stierle, F. Renner, R. Streitel, and H. Dosch, Phys. Rev. B **64**, 165413 (2001).
[36] L. Jurczyszyn, A. Krupski, S. Degen, B. Pieczyrak, M. Kralj, C. Becker, and K. Wandelt, Phys. Rev. B **76**, 045101 (2007).
[37] V. Blum, C. Rath, G. Castro, M. Kottcke, L. Hammer, and K. Heinz, Surf. Rev. Lett. **3**, 1409 (1996).
[38] M. Wuttig, Y. Gauthier, and S. Blügel, Phys. Rev. Lett. **70**, 3619 (1993).
[39] J. Mathon, Rep. Prog. Phys. **51**, 1 (1988).
[40] M. Marcinkowski, M. Taylor, and F. Kayser, J. Mater. Sci. **10**, 406 (1975).
[41] L. Babout, T. J. Marrow, D. Engelberg, and P. J. Withers, Mat. Sci. Technol. **22**, 1068 (2006).
[42] H. Graupner, L. Hammer, K. Heinz, and D. M. Zehner, Surf. Sci. **380**, 335 (1997).
[43] O. Kizilkaya, I. C. Senevirathne, and P. T. Sprunger, J. Appl. Phys. **101**, 063706 (2007).
[44] B. Pöter, F. Stein, R. Wirth, and M. Spiegel, Z. Phys. Chem. **219**, 1489 (2005).